MEDICAL SCIENCE MONITOR

LAB/IN VITRO RESEARCH

e-ISSN 1643-3750
© Med Sci Monit, 2017; 23: 1043-1054
DOI: 10.12659/MSM.900481

Received: 2016.07.08
Accepted: 2016.07.29
Published: 2017.02.27

Computational Analysis of Intra-Ventricular Flow Pattern Under Partial and Full Support of BJUT-II VAD

Authors' Contribution:
Study Design A
Data Collection B
Statistical Analysis C
Data Interpretation D
Manuscript Preparation E
Literature Search F
Funds Collection G

BF Qi Zhang
CDG Bin Gao
AEG Yu Chang

School of Life Sciences and BioEngineering, Beijing University of Technology, Beijing, P. R. China

Corresponding Author: Chang, e-mail: changyu@bjut.edu.cn

Source of support: This work was partly sponsored by the National Natural Science Foundation of China (Grant No. 11572014, 11272022, 91430215). This work was also sponsored by the BJUT Foundation Fund (015000514312002), BJUT Talent Found (Grant No.2014000020124G045), Advanced Medical Instruments (Grant No. 015000514316003), Beijing Talent Fund (Grant No. 015000514116002), Beijing Municipal Education Commission Fund (Grant No. KM201510005028), and the BJUT Foundation Fund (Grant No. 015000514316007)

Background: Partial support, as a novel support mode, has been widely applied in clinical practice and widely studied. However, the precise mechanism of partial support of LVAD in the intra-ventricular flow pattern is unclear.

Material/Methods: In this study, a patient-specific left ventricular geometric model was reconstructed based on CT data. The intra-ventricular flow pattern under 3 simulated conditions – "heart failure", "partial support", and "full support" – were simulated by using fluid-structure interaction (FSI). The blood flow pattern, wall shear stress (WSS), time-average wall shear stress (TAWSS), oscillatory shear index (OSI), and relative residence time (RRT) were calculated to evaluate the hemodynamic effects.

Results: The results demonstrate that the intra-ventricular flow pattern is significantly changed by the support level of BJUT-II VAD. The intra-ventricular vortex was enhanced under partial support and was eliminated under full support, and the high OSI and RRT regions changed from the septum wall to the cardiac apex.

Conclusions: In brief, the support level of the BJUT-II VAD has significant effects on the intra-ventricular flow pattern. The partial support mode of BJUT-II VAD can enhance the intra-ventricular vortex, while the distribution of high OSI and RRT moved from the septum wall to the cardiac apex. Hence, the partial support mode of BJUT-II VAD can provide more benefit for intra-ventricular flow pattern.

MeSH Keywords: Heart-Assist Devices • Hemodynamics • Ventricular Remodeling

Full-text PDF: http://www.medscimonit.com/abstract/index/idArt/900481

3893 — 9 33

Indexed in: [Current Contents/Clinical Medicine] [SCI Expanded] [ISI Alerting System] [ISI Journals Master List] [Index Medicus/MEDLINE] [EMBASE/Excerpta Medica] [Chemical Abstracts/CAS] [Index Copernicus]

Background

Left ventricular assist devices (LVADs) have become a very important treatment method for heart failure [1]. Clinical studies have confirmed that the use of LVAD can improve patient health and quality of life, and significantly reduced the mortality rate of patients with cardiac failure [2]. Along with the development of LVAD, partial support and full support, considered as main support modes of LVAD, are widely used in clinical practice, and their hemodynamic effects on the left ventricular hemodynamics have been attracted increasing attention. Although the LVAD under full support has been proved to significantly improve left ventricular function (e.g., achieving significant unloading performance [3], reducing myocardial oxygen consumption [4], and changing the distribution of wall shear stress (WSS) and vortex [5]), complications involving aortic valve fusion [6] and myocardial atrophy [7] have been reported. To solve these problems, partial support, as an alternative approach, was designed and studied widely. Meyns et al. were the first to study the safety and efficacy of the partial support mode [8]. It is reported that LVAD under partial support mode can provide partial hemodynamic support and its use is associated with significantly improved hemodynamics. Currently, LVAD under partial support has been proved to has positive effects, not only on maintaining the normal function and structure of the aortic valve [9], but also on improving both myocardial unloading and the residence times of blood in the left ventricle [10]. These studies demonstrated that, compared with full support mode, LVAD under partial support can achieve better performance in improving cardiac function recovery and aortic valve function. We hypothesized that their different hemodynamic effects on the left ventricular flow pattern may be one of the key reasons for this. However, the precise mechanism was still unclear.

BJUT-II VAD (previously called an intra-aorta pump), which was developed autonomously by the artificial heart research group at Beijing University of Technology, is a novel LVAD [11]. Unlike traditional LVADs, BJUT-II VAD, which is implanted between the aortic root and aortic arch to avoid damage to the aortic valve, is in series with the native heart (Figure 1). BJUT-II VAD has eliminated the percutaneous wires used to drive the pump by traditional LVAD. The elimination of percutaneous wires significantly reduces the incidence of infection. Research on the control strategies [12–16], support modes [17], and hemodynamic effects [18] of BJUT-II VAD have been reported. The structure of the BJUT-II VAD makes it suitable for long-term support. Hence, it is important to clarify the hemodynamic effect of varied support modes of BJUT-II VAD on the left ventricular flow pattern.

The aim of this investigation was to clarify differences in hemodynamic effect of BJUT-II VAD between partial support and full support on the intra-ventricular blood flow pattern. In order to clarify this mechanism, FSI simulations were conducted. A patient-specific left ventricular geometric model was constructed according to the CT data. Three conditions were designed as the boundary conditions: “heart failure”, “partial support”, and “full support”. The blood flow pattern, wall shear stress (WSS), time-average wall shear stress (TAWSS), oscillatory shear index (OSI), and relative residence time (RRT) were calculated to evaluate the hemodynamic effects.

Material and Methods

The reconstruction of left ventricular model

The use of the data for this study was approved by the local ethics committee, and a consent waiver was granted because

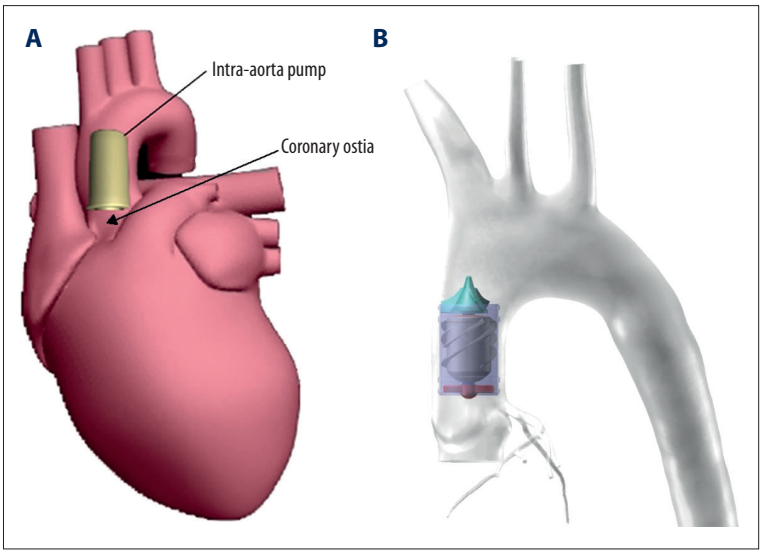

Figure 1. The scheme of BJUT-II VAD and the relationship between the pump and the coronary ostia.

Indexed in: [Current Contents/Clinical Medicine] [SCI Expanded] [ISI Alerting System] [ISI Journals Master List] [Index Medicus/MEDLINE] [EMBASE/Excerpta Medica] [Chemical Abstracts/CAS] [Index Copernicus]

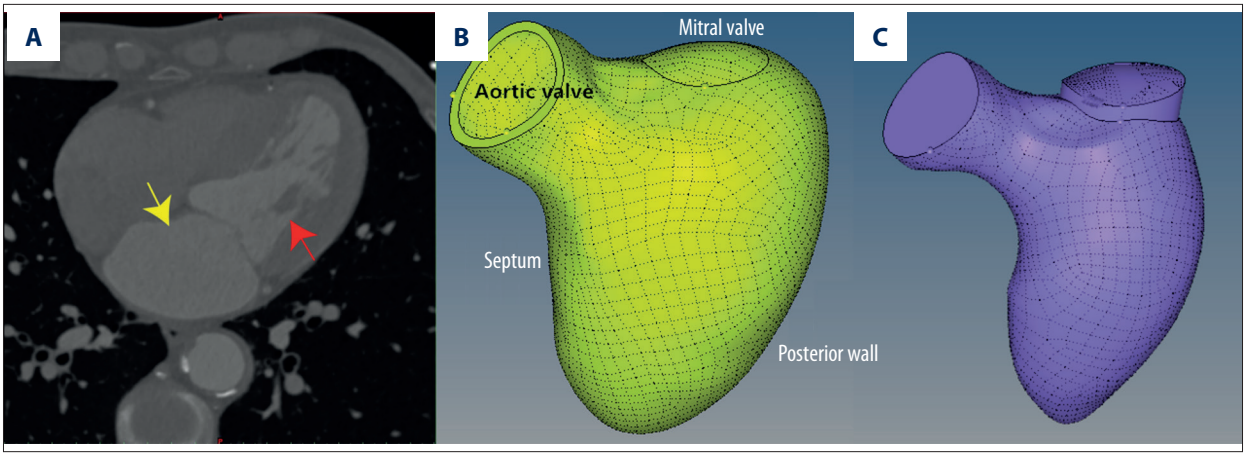

Figure 2. The geometric model of the left ventricle. (**A**) Is the CT scan data of the left ventricle, including left ventricle (red arrow) and left atrium (yellow arrow); (**B**) Is the structure model of the left ventricle; (**C**) Is the fluid model of the blood in the left ventricle.

we only used clinical imaging data. We extracted 3D geometric information from CT scan data from a patient with NYHA III heart failure (Figure 2A). The CT scan was performed for clinical reasons, with electrocardiogram-gating. The images were at 0.5-mm slice thickness, with a 0.3-mm increment, and with a 512×512 pixels. The 3D patient-specific anatomical model was constructed by using these image segmentations and by using commercial 3D reconstruction software MIMICS (Materialise, Belgium) to provide the stereolithographic files (STL format), after which the model was processed using Geomagic software (Geomagic, USA) to obtain better surface quality, smoothing the left ventricle and the blood within it (Figure 2B, 2C). The mitral valve and aortic valve were designed as circles with diameters of 26 mm. According to the results of clinical measurement, the left ventricular volume of this model was about 110 ml.

Meshing generation

Both geometric models were meshed by using a grid generator Hypermesh (Altair, USA) and then transferred into ADINA FSI software. To determine the appropriate number of grids for this work, grid independency tests, targeting the outlet mean pressure as measures, were conducted. The results demonstrate that 1.08 million tetrahedral elements (there were 491,608 grids in the structure model of the left ventricle and 526,532 grids in the fluid model of the blood) are sufficient for this study (Figure 3).

Numerical scheme of FSI

The fundamental conditions applied to the fluid-structure interaction were the dynamic condition (1) and the kinematic condition (2)

$$n \cdot \tau_f = n \cdot \tau_s \quad (1)$$

$$d_f = d_s \quad (2)$$

Where d_f and d_s represents the displacement of blood and left ventricular wall, respectively. τ_f and τ_s is the stress imposed on the blood and left ventricular wall, respectively. n denotes the normal interface.

For the fluid flow part, Navier-Stokes equations were used based on ALE formulation, which can be obtained through replacing the convective velocity in the standard Navier-Stokes equations by the relative velocity to the moving mesh, as the equation (3)

$$\frac{\partial}{\partial t}\int_V \rho dV + \int_S \rho(v - v_b)\cdot n dS = 0 \quad (3)$$

$$\frac{\partial}{\partial t}\int_V \rho v dV + \int_S (\rho v(v - v_b) + pI - \tau)\cdot n dS = 0 \quad (4)$$

Where ρ represents the fluid density, v is the velocity vector of fluid in a fixed coordinate system, v_b denotes the velocity vector of the boundary S of control volume, and n represents the normal external to this boundary. p denotes the pressure.

When equations (3) and (4) are discretized on moving mesh by a Finite Volume Method (FVM) scheme, a system of nonlinear equations for fluid can be expressed as

$$F_f[X_f; d(X_s)] = 0 \quad (5)$$

In which X_f and X_s are the solution vectors for blood and left ventricular wall, respectively.

In this work, ADINA commercial software was chosen to solve this problem, which used the direct coupling approach to solve

Indexed in: [Current Contents/Clinical Medicine] [SCI Expanded] [ISI Alerting System] [ISI Journals Master List] [Index Medicus/MEDLINE] [EMBASE/Excerpta Medica] [Chemical Abstracts/CAS] [Index Copernicus]

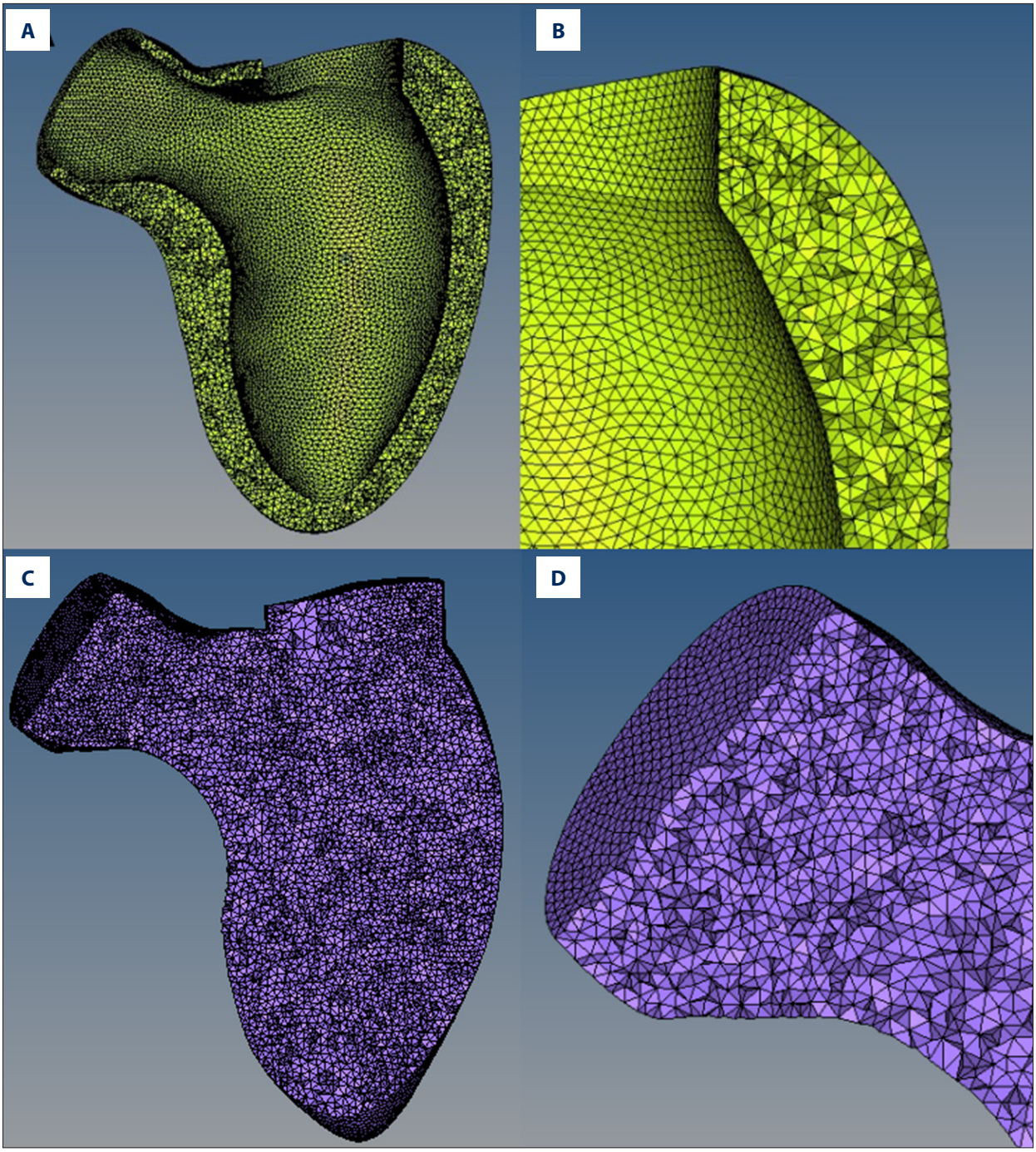

Figure 3. The grid of structure model of left ventricle and the fluid model of blood in the left ventricle.

the FSI problem, confirmed to significantly improve the convergence property and accuracy.

The determination of myocardial property

The key problem is to obtain the correct spatial and temporal distribution of blood flow pattern within the left ventricle, which is consistent with the realistic intra-ventricular flow pattern. The key point is to determine a time-dependent Young's modulus of the left ventricular wall, referred to as the time-dependent Young's modulus curve. The time-dependent Young's modulus used here is an artifice to approximate the change of the left ventricular wall elastic property during the whole cardiac cycle [19]. The details on this process were reported by Cheng et al., and the time-dependent Young's modulus curve used in this work was reported by Hassaballah et al. [20] and is shown in Figure 4A.

Indexed in: [Current Contents/Clinical Medicine] [SCI Expanded] [ISI Alerting System] [ISI Journals Master List] [Index Medicus/MEDLINE] [EMBASE/Excerpta Medica] [Chemical Abstracts/CAS] [Index Copernicus]

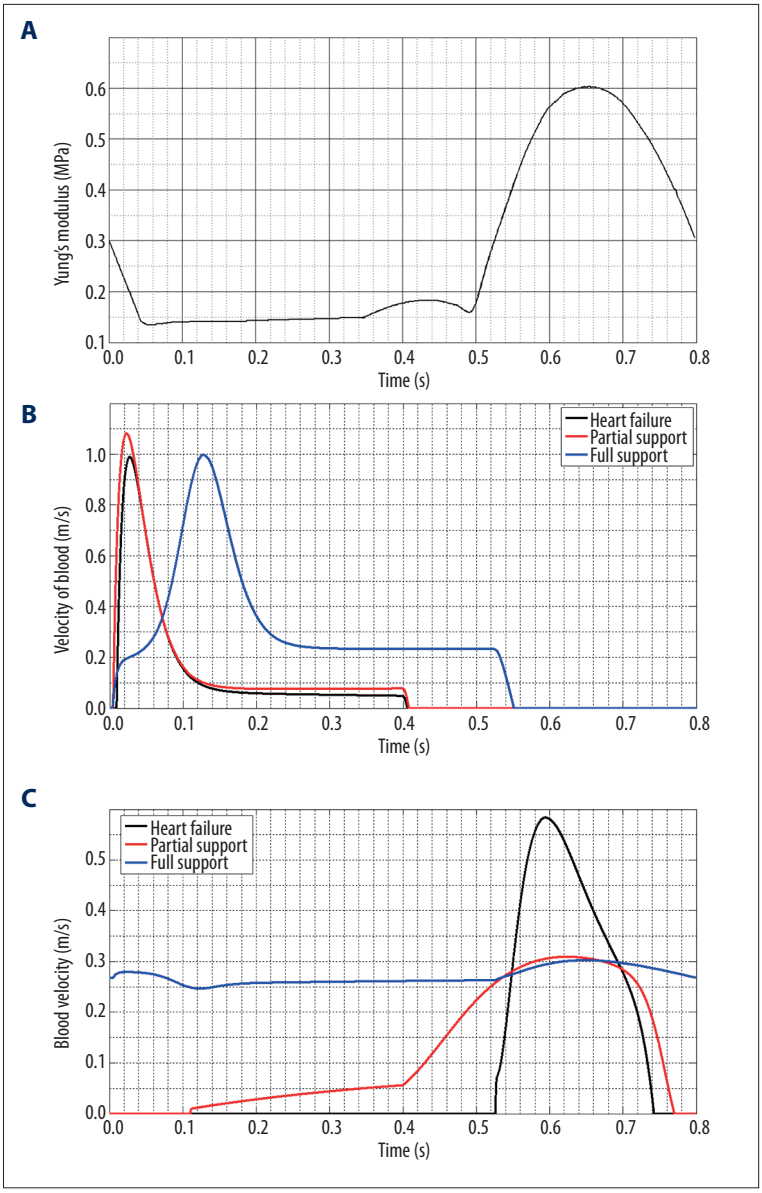

Figure 4. The boundary condition in the FSI simulations. (**A**) Is the Young's modulus curve; (**B**) Is the inlet boundary conditions used in the FSI simulations; (**C**) Is the outlet boundary condition used in the FSI simulations.

The description of support modes

In this work, 2 support modes, referred to as partial support and full support, were designed to compare their hemodynamic effects on the left ventricular blood flow pattern. In addition, the hemodynamic states within the left ventricle of heart failure patients without LVAD support were calculated as the control group. The first support mode is referred to as partial support, under which the aortic valve could open periodically, while the duration of aortic valve opening was longer than that without support by LVAD. The second support mode is referred to as full support, in which the aortic valve was kept opening during the whole cardiac cycle due to the BJUT-II VAD continuously pumping the blood flow from the left ventricle into the ascending aorta.

Boundary conditions

In this study, the physiological velocity data under 3 conditions were used as the boundary conditions for FSI simulation. The boundary conditions are derived from a lumped parameter model [21], of which the accuracy is validated by clinical data. This lumped parameter model consists of the left atrial, left ventricle, LVAD, systemic circulatory system, right atrial, right ventricle, and pulmonary circulatory system. In this study, the blood velocity at the mitral valve and aortic valve was used as the inlet and outlet boundary condition, respectively (Figure 4B, 4C).

Indexed in: [Current Contents/Clinical Medicine] [SCI Expanded] [ISI Alerting System] [ISI Journals Master List] [Index Medicus/MEDLINE] [EMBASE/Excerpta Medica] [Chemical Abstracts/CAS] [Index Copernicus]

Numerical setting

In this work, the blood is assumed to be a homogeneous, incompressible, and Newtonian fluid, of which the density and viscosity is set at 1050 kg/m^3 [22] and 0.0035 Pa•s [23], respectively. The cardiac cycle was set at 0.8 s and the time step length was 2.0 ms. In this work, the simulation was started from the diastolic phase, and the duration of diastolic phase and systolic phase was 0.5 s and 0.3 s, respectively. To accurately evaluate the vortex in the left ventricle, the k-e turbulence model was used in this work. Three cardiac cycles were calculated to obtain stable results independent from initialization and the hemodynamic parameters in the 3rd cardiac cycles have been extracted for hemodynamic analysis and for evaluating the thrombi distribution. The convergence precision in this study was set at 10^{-3}.

Hemodynamic analysis

In order to evaluate the hemodynamic effects of the 3 support conditions on the blood flow and left ventricular wall, the time-average wall shear stress (TAWSS), oscillatory shear index (OSI), and relative resident time (RRT) were calculated.

To access the hemodynamic effects of the blood flow in the left ventricle, the TAWSS was calculated as equation (6)

$$TAWSS=\frac{1}{T}\int_0^T|\tau w|dt \quad (6)$$

Where τ_W is the wall shear stress. T represents the cardiac cycle.

The OSI [24] is defined as the equation (7)

$$OSI=0.5\left(1-\frac{\left|\int_0^T \tau_W dt\right|}{\int_0^T \tau_W dt}\right) \quad (7)$$

The RRT [24] is defined as the equation

$$RRT=\frac{1}{(1-2OSI)\cdot TAWSS} \quad (8)$$

Results

In order to evaluate the hemodynamic effects of varied support mode on the left ventricular flow pattern, the intra-ventricular blood flow pattern, time-average wall shear stress (TAWSS), time-average WSS gradient (TAWSSG), oscillatory shear index (OSI), and relative resident time (RRT) are illustrated in Figures 5–9.

The streamlines of blood in the left ventricle

Figure 5 illustrates the streamlines of blood in the left ventricle in the conditions of heart failure, partial support, and full support. Based on it, the transient flow structure in the left ventricle under these 3 conditions could be described as follows. During the diastolic phase, a strong fill jet is generated from the mitral valve to the left ventricular chamber. Driven by this, a vortex ring is formed at the base of the left ventricle in heart failure and partial support (for heart failure at 0.05 s *vs.* partial support at 0.04 s). Along with the progress of left ventricular diastolic phase, the vortex ring enlarges and travels smoothly towards to the middle of left ventricular cavity at 0.10 s. Later on, during the diastasis, the vortex ring reaches the middle of the left ventricular cavity and the vortex strength under both conditions is significantly weakened (0.25 s). Note that for heart failure, the vortex ring was hardly observed during the diastasis. However, the flow pattern in the left ventricle under full support is quite different from the other conditions. During the whole diastolic phase, no obvious vortex ring can be observed.

The WSS of the left ventricular wall

Figure 6 illustrates the distribution of TAWSS in the 3 conditions. Figure 6A and 6D show the distribution of TAWSS of a heart failure patient without LVAD support. Figure 6B and 6E show the distribution of TAWSS in partial support. Figure 6C and 6F show the distribution of TAWSS in full support, showing that the TAWSS distribution differs depending on the support mode of LVAD. For Figure 6A and 6D, a relatively high TAWSS region was located from the posterior wall around the mitral valve to the septum wall (the mean value of TAWSS is approximately 0.12 Pa). In contrast, a relatively low TAWSS region was observed around the cardiac apex (the mean value of TAWSS is approximately 0 Pa), and the mean value of high TAWSS was enlarged along with the increase of support level of LVAD (partial support 0.17 Pa *vs.* full support 0.23 Pa) (Figure 6B, 6C, 6E, 6F). In addition, due to the increase of blood velocity across through the mitral valve, the value and area of high TAWSS in full support was significant larger than that in partial support and heart failure conditions. Moreover, the area of relatively low TAWSS was also enlarged as the increase of support level of LVAD.

The WSSG of the left ventricular wall

Figure 7 shows the distribution of TAWSSG of left ventricular wall in the 3 conditions. Figures 7A and 7D show the distribution of TAWSSG of heart failure patient without LVAD support. Figures 7B and 7E represent the distribution of TAWSSG in partial support, and Figure 7C and 7F show the distribution of TAWSSG in full support. The distribution of TAWSSG differed depending on the change in support level of LVAD. For all of these 3 conditions, the relatively high TAWSSG regions were all located around the mitral valve and aortic valve. In contrast, the relatively low TAWSSG regions were all near the

Indexed in: [Current Contents/Clinical Medicine] [SCI Expanded] [ISI Alerting System] [ISI Journals Master List] [Index Medicus/MEDLINE] [EMBASE/Excerpta Medica] [Chemical Abstracts/CAS] [Index Copernicus]

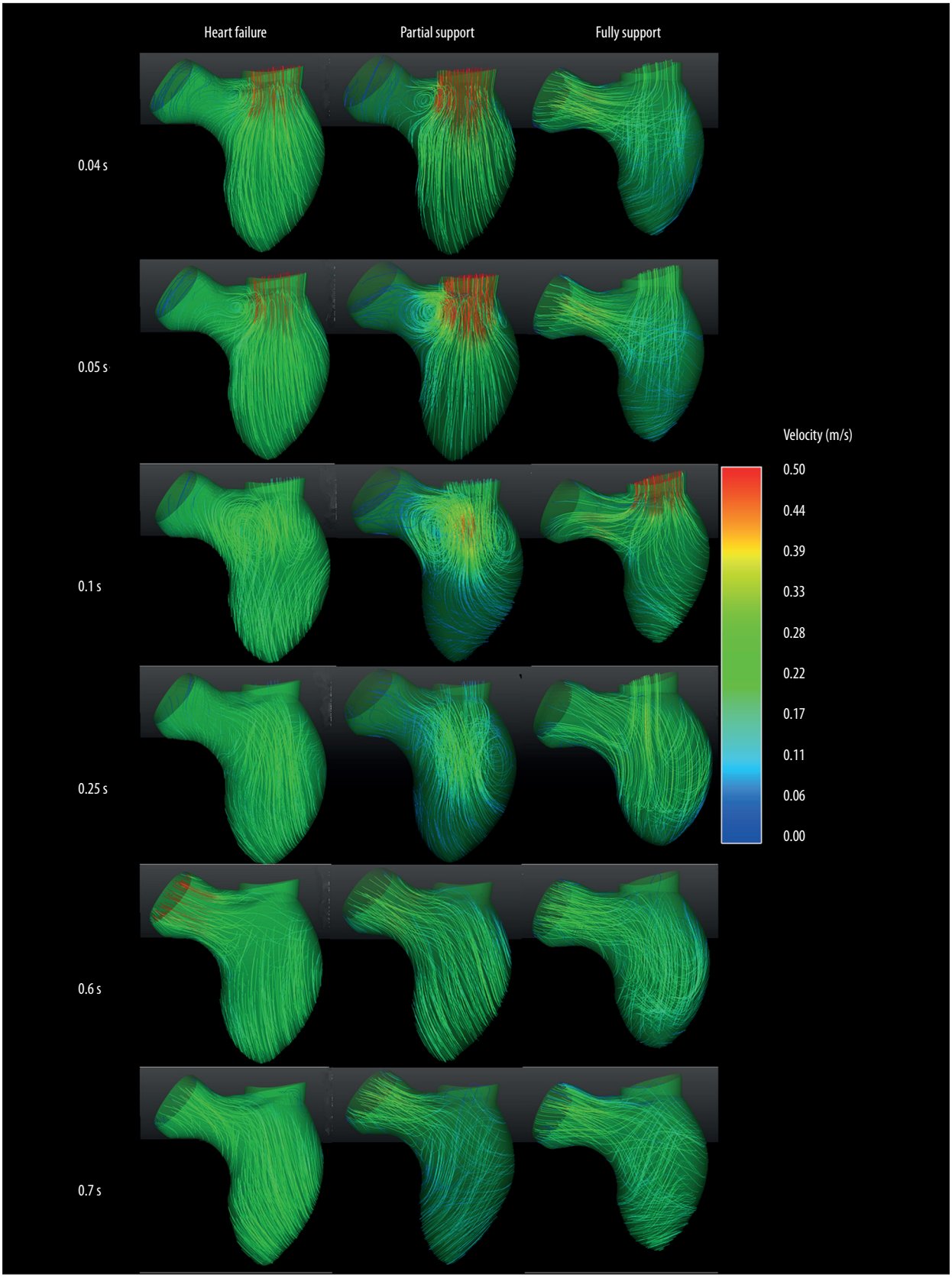

Figure 5. The streamline curve of blood in the left ventricle.

Indexed in: [Current Contents/Clinical Medicine] [SCI Expanded] [ISI Alerting System] [ISI Journals Master List] [Index Medicus/MEDLINE] [EMBASE/Excerpta Medica] [Chemical Abstracts/CAS] [Index Copernicus]

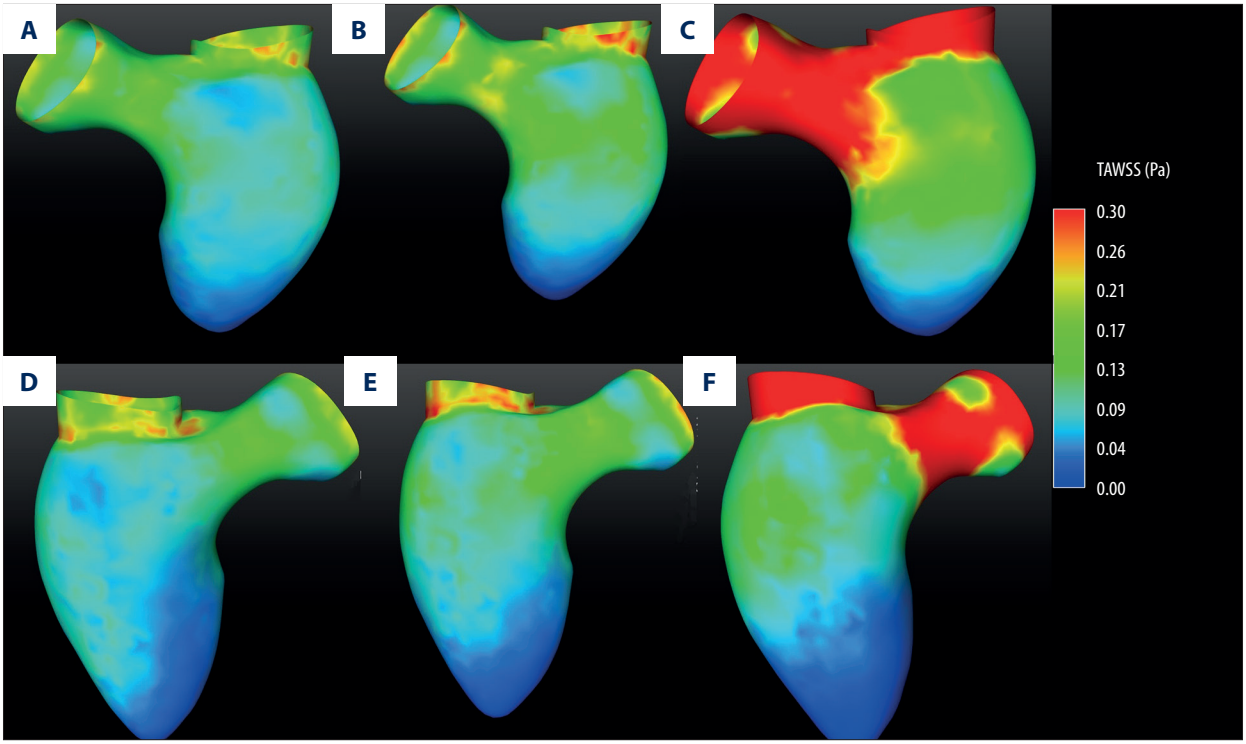

Figure 6. The distribution of TAWSS under the 3 simulated conditions. (**A, D**) Are the distribution of TAWSS of heart failure without LVAD support. (**B, E**) Are the distribution of TAWSS under partial support of LVAD. (**C, F**) Are the distribution of TAWSS under full support of LVAD.

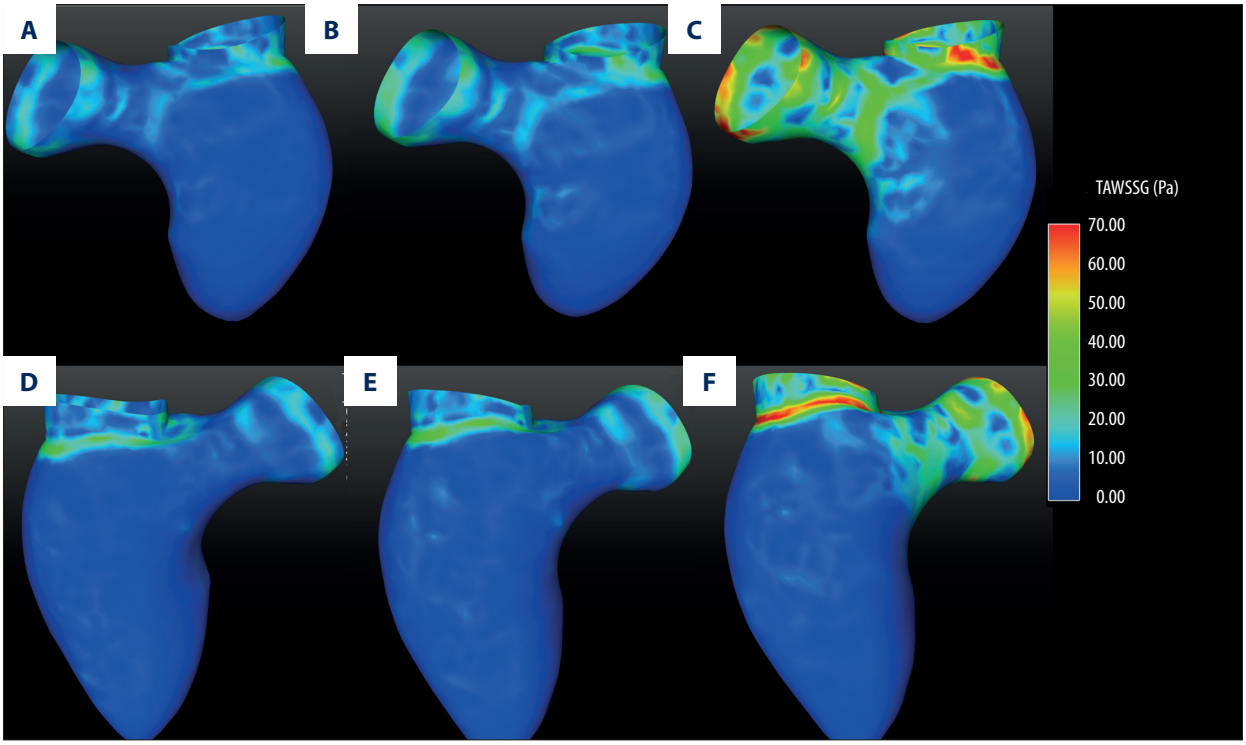

Figure 7. The distribution of TAWSSG under the 3 simulated conditions. (**A, D**) Show the distribution of TAWSSG of a heart failure patient without LVAD support. (**B, E**) Show the distribution of TAWSSG in partial support. (**C, F**) Show the distribution of TAWSSG under full support.

Indexed in: [Current Contents/Clinical Medicine] [SCI Expanded] [ISI Alerting System] [ISI Journals Master List] [Index Medicus/MEDLINE] [EMBASE/Excerpta Medica] [Chemical Abstracts/CAS] [Index Copernicus]

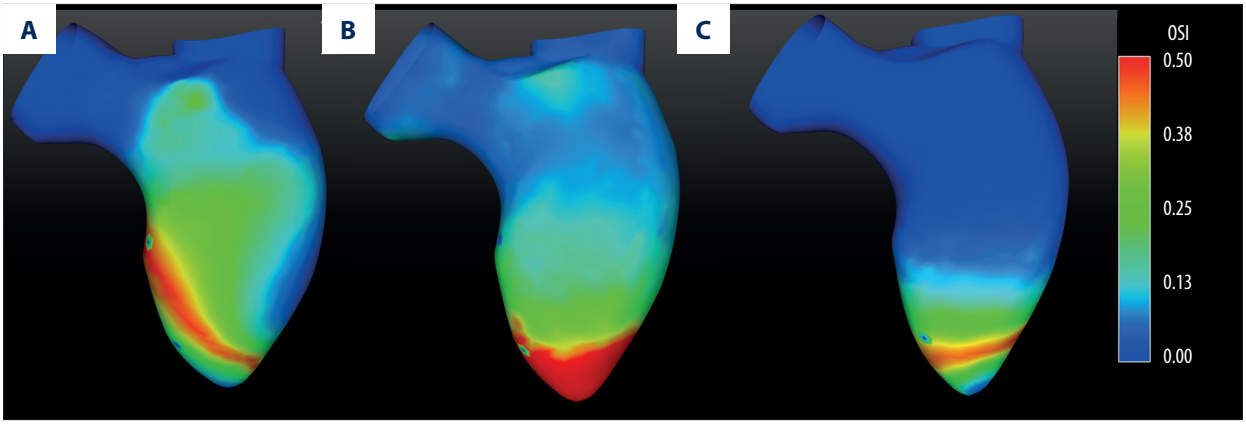

Figure 8. The distribution of OSI of the left ventricular wall. (**A**) Is the distribution of OSI under heart failure; (**B**) Is the distribution of OSI under partial support; and (**C**) Is the distribution of OSI under full support.

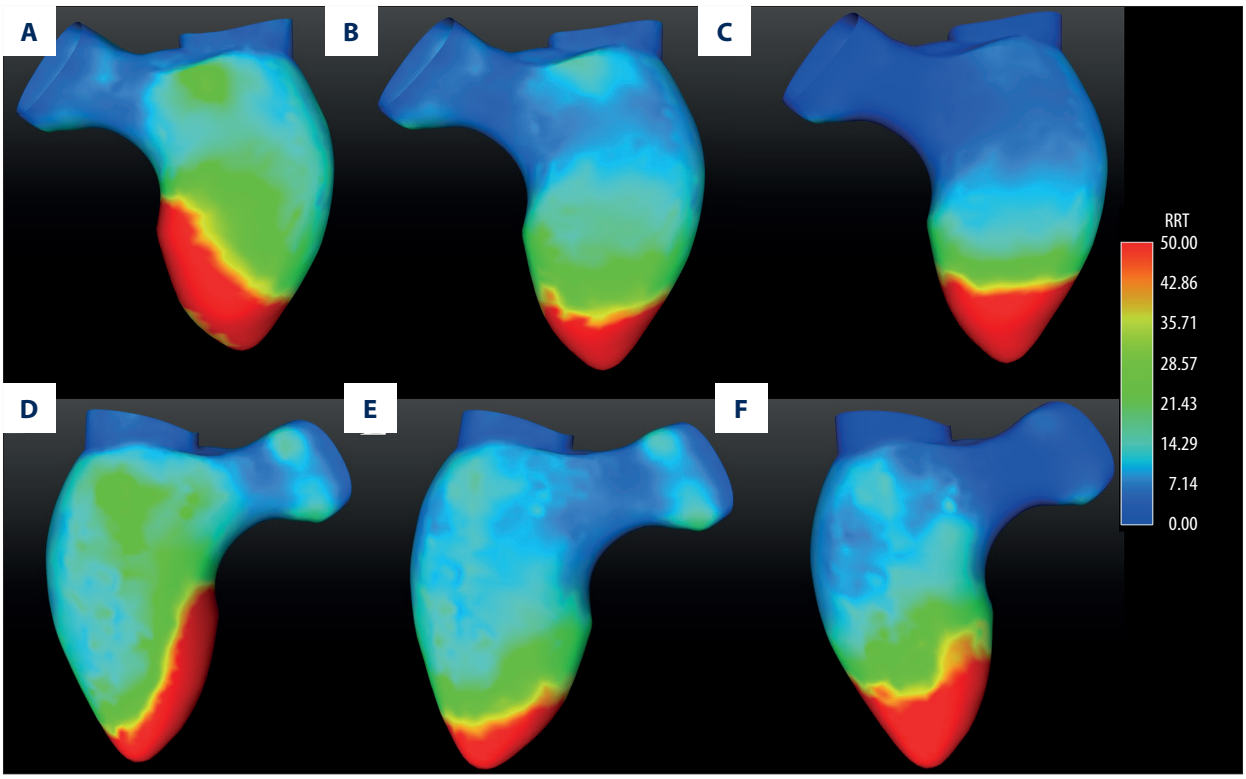

Figure 9. The distribution of RRT in the 3 simulated conditions. (**A, D**) Are the distribution of RRT under heart failure; (**B, E**) Are the distribution of RRT under partial support; (**C, F**) Are the distribution of RRT under full support.

cardiac apex. Moreover, the value of TAWSSG was increased along with the increase of support level of LVAD. Figure 7 shows that the maximum value of high TAWSSG in full support was significant higher than that in partial support and heart failure (heart failure about 30 Pa/m *vs.* partial support 40 Pa/m *vs.* full support larger than 70 Pa/m).

The distribution of OSI of the left ventricular wall

Figure 8 shows the distribution of OSI of the left ventricular wall under the 3 conditions. Figure 8A illustrates the distribution of OSI of the left ventricular wall under heart failure. Figure 8B shows the OSI distribution of the left ventricular wall under partial support. Figure 8C illustrates the OSI distribution of the left ventricular wall under full support. The support level significantly affects the distribution of OSI. When the heart failure patients were not supported by LVAD, the high OSI region

Indexed in: [Current Contents/Clinical Medicine] [SCI Expanded] [ISI Alerting System] [ISI Journals Master List] [Index Medicus/MEDLINE] [EMBASE/Excerpta Medica] [Chemical Abstracts/CAS] [Index Copernicus]

was located at the septum wall, where the maximum value of OSI was approximately 0.45 (Figure 8A). However, when the patients were supported by LVAD, the distribution of OSI was significantly changed. For partial support, the high OSI region, observed in heart failure, disappeared (Figure 8B). The maximum value of OSI was 0.32 at the region of the cardiac apex, and the area of high OSI region was also significantly reduced compared with that in heart failure patients. For full support, the high OSI region moved upward (Figure 8C) and its maximum value increased to 0.40. Moreover, the area of the high OSI region was larger than that under partial support, and was smaller than that under heart failure.

The distribution of RRT of the left ventricular wall

Figure 9 shows the distribution of RRT of the left ventricular wall in the 3 conditions. Figure 9A and 9D illustrate the distribution of RRT of the left ventricular wall in heart failure. Figure 9B and 9E show the RRT distribution of the left ventricular wall in partial support. Figure 9C and 9F illustrate the RRT distribution of the left ventricular wall in full support, showing that the distribution of RRT was significantly affected by the support conditions. For heart failure, the high RRT region was located at the septum wall, where the maximum value of RRT was larger than 50. For partial support and full support, the high RRT region moved from the septum wall to the cardiac apex and the region area was reduced compared to that in heart failure.

Discussion

The results presented in this work provide detailed analysis of the left ventricular hemodynamic states under different support levels (heart failure, partial support, and full support conditions) based on patient-specific left ventricular geometrics. Significant variations in the left ventricular flow pattern and hemodynamic effects imposed on the left ventricular wall were observed along with the changes in varied support levels. These results provided insight into how the support level of LVAD affects the intra-ventricular hemodynamic states and their potential effects on the cardiac function.

Partial mechanical circulatory support devices are attracting increasing research attention. As the special relationship between pump outflow and native heart flow, a better understanding of the induced flow alterations is warranted. Karmonik et al. first studied the hemodynamic effect of a partial mechanical circulatory support device (Circulite Synergy Micro Pump) on the hemodynamic states in the aorta [33]. They demonstrated that CFD in combination with clinical CTA images and patient-specific inflow boundary conditions are capable of reproducing flow features in the aorta and adjacent arteries. In this investigation, we found that the hemodynamic effect of partial support device on the aorta is quite different from that of a full support device, and the CFD is a useful method for researchers to use in clarifying the differences between them. Similarly, it is reasonable to assume that the intra-ventricular blood flow pattern is also changed. The present study is the first to clarify the intra-ventricular flow pattern by using the FSI approach.

The vortex was considered as a very important hemodynamic characteristic in the left ventricle. It is a consequence of left ventricular chiral geometry and the interaction of the filling jet with the left ventricle walls [25]. The vortex is relatively long-standing and inertial flow structures are capable of entraining fluid and decreasing pressure in their vicinity without an energetic loss during diastolic phase. Hence, a leading vortex could transport more blood than an equivalent straight jet of blood [26]. In addition, the vortex also contributed to improving the blood mixture in the left ventricle [10]. The stronger vortex in the left ventricle has less stagnation time of the blood and could prevent thrombosis in the left ventricle. Although the role of the vortex on the left ventricular hemodynamic states have been well characterized *in vivo* and *in vitro* [27–29], the present study is the first to evaluate the effects of different support modes (heart failure, partial support, and full support) on the intra-ventricular hemodynamic states. For heart failure, the strength and formation time of the vortex were reduced compared with that in a healthy heart, due to the reduction of the blood velocity across through the mitral valve (Figure 5 left column), consistent with previous studies [30,31]. For heart failure patients, the cardiac function was significantly impaired, which could reduce the blood velocity across through the mitral valve, and this change led to the weakness and reduction of formation time of vortex in the left ventricle during the diastolic phase. This change will reduce the level of blood mixture and may result in thrombosis in the left ventricle. When the patient was supported by LVAD, the vortex in the left ventricle was quite different from that that in heart failure. For partial support, the strength of the vortex was significantly increased compared with that in heart failure (Figure 5B middle column). In addition, the area of the vortex was also enlarged (located at the aortic root in heart failure *vs.* in the whole ventricular cavity in partial support) and the vortex formation time increased (heart failure 0.1 s *vs.* partial support 0.25 s). This change might enhance the level of blood mixture and reduce the energetic cost to the heart, which may prevent thrombosis and decrease the work load. This may promote cardiac function recovery. Interesting, the effects of partial support and full support on the vortex were quite different from each other. In full support mode, the vortex was not observed during the whole cardiac cycle (Figure 5 right column), resulting from the blood being continuously jetted from aortic valve by LVAD during the whole cycle. This phenomenon may result in

Indexed in: [Current Contents/Clinical Medicine] [SCI Expanded] [ISI Alerting System] [ISI Journals Master List] [Index Medicus/MEDLINE] [EMBASE/Excerpta Medica] [Chemical Abstracts/CAS] [Index Copernicus]

a larger stagnant blood region near the cardiac apex because little blood could reach the cardiac apex. Hence, the thrombosis near the cardiac apex may be more affected by BJUT-II VAD under full support than in partial support mode. This result was different from the finding reported by Wong et al. [32], who found that the vortex circulation and kinetic energy increased with LVAD speed and a region of fluid stasis formed near the aortic valve. This difference resulted from the different implanted location of the LVAD. In Wong's work, the LVAD bypassed with the native heart, which means the inflow cannula of LVAD was anastomosed at the cardiac apex. In this situation, more blood flow would move towards to the cardiac apex along with the increase of LVAD support level, which results in the increased vortex circulation and kinetic energy and eliminated the blood stagnant region. In contrast, BJUT-II VAD was implanted into the ascending aorta, which is in series with the native heart, and the blood flow was through the aortic valve and then enters the BJUT-II VAD. Hence, along with the increase of support level of BJUT-II VAD, more blood entering from the mitral valve would directly go through the aortic valve by BJUT-II VAD. In this situation, the stagnant blood region was observed near the cardiac apex, and its area increased along with the increase of support level of BJUT-II VAD.

Limitations

As with any numerical simulation, the FSI results present a simplification of reality in which only the most pertinent features are considered. In this investigation, a time-dependent linear elastic material was used to mimic the mechanical property of myocardial issue. In addition, the hyperelastic property of myocardial issue was not included in this study. Although the simplifications reduce the accuracy of the results on the myocardial biomechanical property, this study focuses on the intra-ventricular flow pattern. Hence, this simplification will not affect the accuracy of the results of this study.

In this study, the motions of aortic valve and mitral valve have been ignored to reduce the computational cost. The aortic valve motion has been proved to play an important role in blood flow pattern. The aortic valve has significant effects on the aortic blood flow pattern, but not the intra-ventricular blood flow. Hence, it is reasonable to ignore its motion.

In this study, only a patient-specific left ventricular model has been reconstructed to be used in this investigation. Although the number of samples is enough for clarify this hemodynamic effect by using numerical approach, it is obviously insufficient for clinical application. This may cause inaccuracies in the reconstructed computational models, making it difficult to come to plausible conclusions regarding the advantageous clinical applications of this design. Hence, more patient-specific left ventricular models need to be reconstructed and analyzed by using the FSI approach, and then these results need to be statistically analyzed to obtain a more precise mechanism that could provide more useful information to clinical surgeons.

Conclusions

An FSI study was conducted to investigate the hemodynamic effect of different support levels of BJUT-II VAD on intra-ventricular flow characteristics. A patient-specific left ventricular geometric model was reconstructed based on the CT data. The FSI approach was employed to calculate the intra-ventricular flow characteristics. The study demonstrated that the intra-ventricular flow pattern is significantly changed by the support level of BJUT-II VAD. An obvious vortex was not seen in the left ventricle in full support, but it was obvious in heart failure and partial support. In addition, for WSS distribution, the value and area of high TAWSS under full support was significantly larger than that under partial support mode and heart failure mode. The area of relative low TAWSS was also enlarged with increased support level of LVAD. In addition, under BJUT-II VAD support, the location of high OSI area changed from the left ventricular septum wall to the cardiac apex. The area of high RRT was also reduced compared to that in heart failure.

References:

1. Kitada S, Schulze PC, Jin Z et al: Comparison of early versus delayed timing of left ventricular assist device implantation as a bridge-to-transplantation: An analysis of the UNOS dataset. Int J Cardiol, 2016; 203: 929–35
2. Slaughter MS, Pagani FD, Rogers JG et al: Clinical management of continuous-flow left ventricular assist devices in advanced heart failure. J Heart Lung Transplant, 2010; 29(4): S1–39
3. Cox LG, Loerakker S, Rutten MC et al: A mathematical model to evaluate control strategies for mechanical circulatory support. Artif Organs, 2009; 33(8): 593–603
4. Ando M, Takewa Y, Nishimura T et al: Coronary vascular resistance increases under full bypass support of centrifugal pumps – relation between myocardial perfusion and ventricular workload during pump support. Artif Organs, 2012; 36(1): 105–10
5. Yano T, Funayama M, Sudo S et al: Analysis of flow within a left ventricle model fully assisted with continuous flow through the aortic valve. Artif Organs, 2012; 36(8): 714–23
6. Hata H, Fujita T, Ishibashi-Ueda H, et al: Pathological analysis of the aortic valve after long-term left ventricular assist device support. Eur J Cardiothorac Surg, 2014; 46(2): 193–97
7. Oriyanhan W, Tsuneyoshi H, Nishina T et al: Determination of optimal duration of mechanical unloading for failing hearts to achieve bridge to recovery in a rat heterotopic heart transplantation model. J Heart Lung Transplant, 2007; 26(1): 16–23
8. Meyns BP, Simon A, Klotz S et al: Clinical benefits of partial circulatory support in New York Heart Association Class IIIB and Early Class IV patients. Eur J Cardiothorac Surg, 2011; 39(5): 693–98

Indexed in: [Current Contents/Clinical Medicine] [SCI Expanded] [ISI Alerting System] [ISI Journals Master List] [Index Medicus/MEDLINE] [EMBASE/Excerpta Medica] [Chemical Abstracts/CAS] [Index Copernicus]

9. Martina JR, Schipper ME, de Jonge N et al: Analysis of aortic valve commissural fusion after support with continuous-flow left ventricular assist device. Interact Cardiovasc Thorac Surg, 2013; 17(4): 616–24
10. McCormick M, Nordsletten D, Lamata P et al: Computational analysis of the importance of flow synchrony for cardiac ventricular assist devices. Comput Biol Med, 2014; 49: 83–94
11. Chang Y, Gao B: Modeling and Identification of an Intra-Aorta Pump. Asaio J, 2010; 56(6): 504–9
12. Chang Y, Gao B: A global sliding mode controller design for an intra-aorta pump. Asaio J, 2010; 56(6): 510–16
13. Gao B, Nie LY, Chang Y et al: Physiological control of intraaorta pump based on heart rate. Asaio J, 2011; 57(3): 152–57
14. Chang Y, Gao B: A model-free adaptive control to a blood pump based on heart rate. Asaio J, 2011; 57(4): 262–67
15. Gao B, Zeng Y et al: a blood assist index control by intraaorta pump: a control strategy for ventricular recovery. Asaio J, 2011; 57(5): 358–62
16. Gao B, Chang Y: An anti-suction control for an intro-aorta pump using blood assistant index. Artif Organs, 2012; 36(3): 275–82
17. Gao B, Chang Y, Xuan Y et al: The hemodynamic effect of the support mode for the intra-aorta pump on the cardiovascular system. Artif Organs, 2013; 37(2): 157–65
18. Xuan Y, Chang Y et al: Hemodynamic simulation study of a novel intra-aorta left ventricular assist device. Asaio J, 2012; 58(5): 462–69
19. Cheng Y, Oertel H, Schenkel T et al: Fluid-structure coupled CFD simulation of the left ventricular flow during filling phase. Ann Biomed Eng, 2005; 33(5): 567–76
20. Hassaballah AI, Hassan MA, Mardi AN et al: An inverse finite element method for determining the tissue compressibility of human left ventricular wall during the cardiac cycle. PLoS One, 2013; 8(12): e82703
21. ZM Song, B Gao et al: Hemodynamic effect of various support modes of continuous flow LVADs on the cardiovascular system: A numerical study. Med SciMonit, 2014; 20: 733–41
22. Khalafvand SS, NG Eyk, Zhong L et al: Fluid-dynamics modeling of the human left ventricle with dynamic mesh for normal and myocardial infarction: Preliminary study. Comput Biol Med, 2012; 42(8): 863–70
23. X Zhao, YJ Liu, F Bai et al: [Numerical study on bilateral bidirectional Glenn shunt.] Journal of Medical Biomechanics, 2012; 27(5): 488–94 [in Chinese]
24. Rikhtegar F, Knight JA, Olgac U et al: Choosing the optimal wall shear parameter for the prediction of plaque location-A patient-specific computational study in human left coronary arteries. Atherosclerosis, 2012; 221(2): 432–37
25. Martínez-Legazpi P, Bermejo J, Benito Y et al: Contribution of the diastolic vortex ring to left ventricular filling. J Am Coll Cardiol, 2014; 64(16): 1711–21
26. Shadden SC, Katija K, Rosenfeld M et al: Transport and stirring induced by vortex formation. J Fluid Mech, 2007; 593: 315–31
27. Pedrizzetti G, La Canna G, Alfieri O et al: The vortex – an early predictor of cardiovascular outcome? Nat Rev Cardiol, 2014; 11(9): 545–53
28. Kanski M, Arvidsson PM, Töger J et al: Left ventricular fluid kinetic energy time curves in heart failure from cardiovascular magnetic resonance 4D flow data. J Cardiovasc Magn Reson, 2015; 17(1): 111
29. Töger J, Kanski M, Arvidsson PM et al: Vortex-ring mixing as a measure of diastolic function of the human heart: Phantom validation and initial observations in healthy volunteers and patients with heart failure. J Magn Reson Imaging, 2015; 43(6): 1386–97
30. Poh KK, Lee LC, Shen L et al: Left ventricular fluid dynamics in heart failure: echocardiographic measurement and utilities of vortex formation time. Eur Heart J Cardiovasc Imaging, 2012; 13(5): 385–93
31. Gharib M, Rambod E, Kheradvar A et al: Optimal vortex formation as an index of cardiac health. Proc Natl Acad Sci USA, 2006; 103(16): 6305–8
32. Wong K, Samaroo G, Ling I et al: Intraventricular flow patterns and stasis in the LVAD-assisted heart. J Biomech, 2014; 47(6): 1485–94
33. Karmonik C, Partovi S, Rengier F et al. Hemodynamic assessment of partial mechanical circulatory support: Data derived from computed tomography angiographic images and computational fluid dynamics. Cardiovasc Diagn Ther, 2015; 5(2): 160–65

Indexed in: [Current Contents/Clinical Medicine] [SCI Expanded] [ISI Alerting System] [ISI Journals Master List] [Index Medicus/MEDLINE] [EMBASE/Excerpta Medica] [Chemical Abstracts/CAS] [Index Copernicus]